Journal of Applied Polymer Science

Role of Poly(lactic acid) in the Phase Transition of Poly(vinylidene fluoride) Under Uniaxial Stretching

Qi Xie, Kai Ke, Wen-Rou Jiang, Wei Yang, Zheng-Ying Liu, Bang-Hu Xie, Ming-Bo Yang

Department of Polymer Processing and Engineering, College of Polymer Science and Engineering, Sichuan University, State Key Laboratory of Polymer Materials Engineering, Chengdu, 610065 Sichuan, China

ABSTRACT: The effect of poly (lactic acid) (PLA) on the crystalline phase transition of poly (vinylidene fluoride) (PVDF) from α- to β-phase under uniaxial stretching for immiscible PVDF/ PLA blends was investigated. The typical sea-island structure in the blends was found to facilitate the necking of PVDF and the transition from α- to β-phase due to the local stress distribution during stretching. The crystalline phase transition of PVDF in the blends is temperature-dependent and is affected by the content of PLA. The highest content of β-phase, F(β), was achieved in the samples stretched at 60°C, while the effect of PLA content on the crystalline phase transition of PVDF is more complex. F(β) increases slightly when the sample with a PLA content no more than 15 wt % is stretched at 60, 80, and 100°C, and decreases sharply for the sample containing 20 wt % PLA; in addition, the sample containing 10 wt % PLA exhibits the highest F(β) no matter what the stretching temperature is. The mechanism of the crystalline phase transition of PVDF during the stretching is interpreted from energy barrier of the transition from α- to β-phase and the morphological structures in the blends. © 2012 Wiley Periodicals, Inc. J. Appl. Polym. Sci. 129: 1686–1696, 2013

KEYWORDS: blends; crystallization; morphology; properties and characterization; structure-property relations

Received 18 September 2012; accepted 23 November 2012; published online 18 December 2012
DOI: 10.1002/app.38873

INTRODUCTION

Deformation of crystalline polymers under uniaxial or biaxial stretching leads to the orientation of molecular chains and even the breakage of crystals, which results in the rearrangement of crystals after the applied stress is removed or compels the chains in the amorphous zone to align. In this process, the crystalline structures are tremendously influenced.[1,2] Interestingly, such a deformation process can also generate phase transition of polymorphous crystalline polymers such as polypropylene,[3,4] poly (butylene terephthalate),[5] nylon 6,[6] poly (lactic acid) (PLA)[7,8] and poly (vinylidene) (PVDF),[9–15] etc, among which PVDF is very attractive because of the relatively large piezoelectric and pyroelectric response determined by its polymorphic crystal forms.

Usually, three main crystalline phases,[16] that is, α-phase, β-phase and γ-phase, can be observed in PVDF, and only β-phase PVDF exhibits piezoelectricity. Consequently, technologies to achieve a high content of β-phase PVDF have been explored for several decades and methods such as electrical field polarization,[17] mechanical drawing,[9–15] crystallization from the solution,[18] epitaxial crystallization on nanofillers,[19,20] etc, have been developed. In these methods, mechanical drawing is generally viewed as a preferred choice to achieve a high content of β-phase PVDF due to its operation convenience and low cost.

The crystalline phase transition by mechanical stretching for neat PVDF and its composites has been widely investigated. Initially, Lando et al.[9] found that drawing PVDF films at 50°C yielded a single phase (form I), while drawing at temperatures between 120 and 160°C yielded a mixture of crystal structures of β phase (form I) and α phase (form II). Later, Matsushige et al.[10] systemically studied the effect of drawing temperature on the α- to β-phase transformation of PVDF and found that the crystalline phase transformation occurred in the necking region for samples deformed by cold-drawing below 130°C, while for samples deformed uniformly without necking at temperatures above 140°C, α-crystals orientated along the drawing direction instead. Later, many studies[11–15] involving various drawing ratios, strain rates and stretching temperatures were carried out, and it has been confirmed that heterogeneous stress distribution plays a significant role in the α- to β-phase transformation and the stretching induced transformation of crystalline phase is strongly influenced by drawing speed, drawing ratio and drawing temperature.

The crystalline phase transition of PVDF also occurs in PVDF blends. Li et al. conducted a series studies on the effect of uniaxial stretching on the crystalline phase transition of PVDF in the PVDF/poly(1, 4-butylene succinate) blends[21] and PVDF/Acrylic rubber blends.[22] The molecules in the amorphous region were found to function as tie molecules to transfer the stress to crystals during stretching, which facilitates the conversion of the chain conformation into that of all-trans β phase. They also found that the interaction between PVDF and polyamide 11 (PA11) played a critical role in the crystallization and orientation of PVDF, and α-, β-crystal coexisted in melt-cooled PVDF/PA11 blends, while β crystals of PVDF maintained the c-axis orientation irrespective of crystallization conditions.[23] The introduction of poly (methyl methacrylate) (PMMA) into PVDF also promotes the formation of β crystals of PVDF. Specially, PVDF/PMMA blend with 10% PMMA stretched at room temperature with a modest deformation rate favored a nearly complete transition of α- and γ- to β-phase.[24]

As a biocompatible polymer, PLA shows great potential in biomedical applications such as implants, structures and drug encapsulations, etc.[25] PLA also exhibits piezoelectricity although its piezoelectric coefficient is lower than PVDF.[26,27] Generally, amorphous poly(L-lactic) (PLLA) shows very weak piezoelectricity but drawing endows PLLA films with piezoelectricity and the piezoelectric constant increases with drawing ratio when the drawing ratio is less than 5.[28]

PVDF/PLA blends have caught the interest of researchers recently. Kaito et al.[29] found that oriented crystallization of α phase of PLLA in PVDF/PLLA blends occurred in the stretched domains of PLLA with diameters of 0.5–0.2 μm and they ascribed it to the heteroepitaxy of the (200)/(110) axes of the α crystals of PLLA along the (201)/(111) axes of the β crystals of PVDF due to lattice matching of d_{100}(PLLA) $\approx 5d_{201}$(PVDF). Chen et al.[30] also found the transition of crystalline phase from α- to β-form of PVDF for the spun PVDF/PLA samples.

It is now known that the formation of necking plays a crucial role in the conversion of α- to β-form of PVDF and the introduction of PLA influences the crystallization and crystalline structures of PVDF. However, the effect of PLA on the deformation of PVDF matrix and the effect of PLA content on the phase transition of PVDF from α- to β-phase for PVDF/PLA blends during stretching are of interest. Aiming at facilitating the deformation of PVDF matrix during uniaxial stretching by the introduction of a second phase with higher deformability at certain temperatures, the crystalline behavior and crystalline phase transition of PVDF in PVDF/PLA blends during stretching in a temperature-controllable chamber were studied.

EXPERIMENTAL

Materials

PVDF resin (FR 901) in the form of powder was obtained from 3F Co. Ltd., Shanghai, China. The weight average molecular weight and polydispersity index (PDI) were 285, 500 g/mol and 1.9, respectively. With a weight average molecular weight of 81, 900 g/mol and a PDI of 2.92, PLA (Revode101) was supplied by Zhejiang Hisun Biomaterials, Taizhou, China.

Sample Preparation

PVDF/PLA blends with 5, 10, 15, 20 wt % of PLA were prepared in a 60 ml mixer of a torque rheometer (XSS-300, Shanghai Kechang Rubber Plastics Machinery Set, Shanghai, P. R. China). To prevent or lessen the degradation of PLA, the powdery PVDF and PLA granules with preset compositions were premixed manually and then were melt mixed for 6 min with a rotation speed of 50 r/min at 190°C. For comparison, neat PVDF and PLA samples were prepared under the same conditions. The blends are designated as FL. For instance, the blend containing 5 wt % PLA was named as FL5. For the uniaxial stretching, the melt mixed samples were compression-molded into sheets at 190°C and 7 MPa, and then cut into dog-bone specimens.

Uniaxial stretching was performed on the dog-bone samples (6 mm width × 20 mm gauge length) on an AGS-J universal testing machine (Shimazu, Japan) equipped with a temperature chamber. After being kept in the temperature chamber for 5 min to achieve thermal equilibrium, the samples were uniaxially stretched at different temperatures (60, 80, and 100°C) with a constant cross-head speed of 5 mm/min to realize a strain of 400%. The strain of the stretched sample was measured from a separation of ink marks at 5 mm interval preprinted on the samples. The samples stretched to preset strain were quenched by ultralow temperature solution in the extension state to freeze the structural characteristics achieved.

Characterizations

The viscoelastic properties were studied using a stress controlled dynamic rheometer AR2000ex (TA, USA), in a parallel plate geometry. The melt mixed samples were compression-molded into disks with the diameter of 25 mm and the thickness of 1.5 mm at 190°C and 7 MPa. The dynamic frequency sweeps were conducted at 190°C under nitrogen atmosphere with a strain of 2% which was within the linear viscoelastic region, and the oscillation frequency range was 0.01–70 Hz.

The molecular vibration spectra of the samples were measured using a Nicolet 6700 FTIR instrument (Nicolet, USA). FTIR-attenuated total reflection (ATR) spectra were recorded from 650 to 4000 cm^{-1} by averaging 32 scans at a resolution of 2 cm^{-1}.

The melting and crystallization behavior were characterized by a Q20 differential scanning calorimeter (DSC) (TA, USA). The unstretched samples were heated to 200°C at a heating rate of 100°C/min, held at 200°C for 5 min to erase the thermal history, and then cooled down to 30°C at a cooling rate of 10 °C / min. Two minutes later, the samples were heated to 200°C again at a heating rate of 10°C/min. The cooling and the second heating curves were recorded. To study the influence of mechanical stretching on the crystalline structures of the samples, a heating scan with a heating rate of 5°C/min was also performed.

Wide-angle X-ray diffraction (WAXD) measurements were performed on a DX-1000 diffractometer at room temperature. Patterns were recorded from 2° to 50° with a scanning speed of 2°/min, using a Cu Kα (0.154 nm) irradiation source of 40 kV and 40 mA.

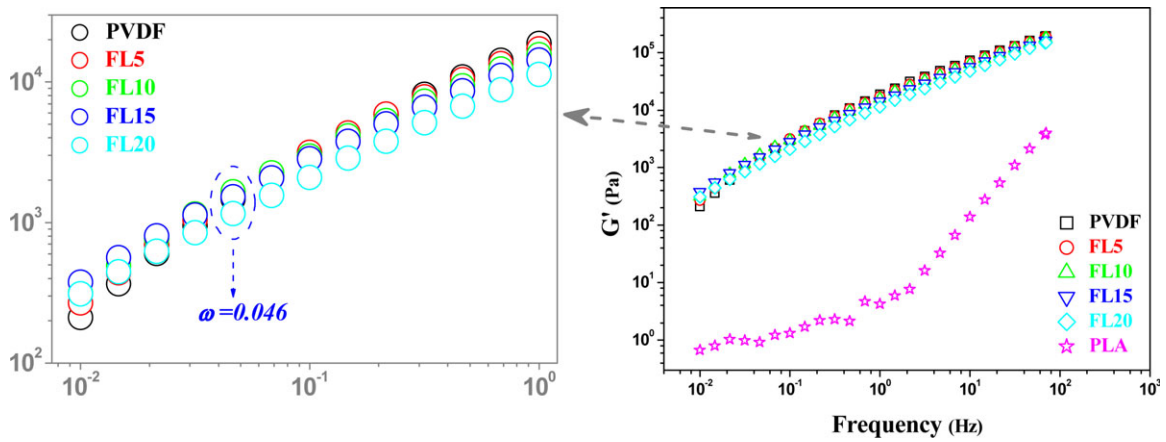

Figure 1. The frequency-dependent storage modulus of PVDF/PLA blends. [Color figure can be viewed in the online issue, which is available at wileyonlinelibrary.com.]

The morphologies of the fractured surface parallel to the drawing direction were observed using a JSM-5900LV scanning electron microscope (SEM, JEOL, Japan) at an accelerating voltage of 20 kV. The samples were left in liquid nitrogen for 40 min and then impact fractured for SEM analysis. The freshly fractured surface was gold sputtered before SEM observation.

RESULTS AND DISCUSSION

Viscoelastic Behaviors and Initial Morphology

For polymer blends, the miscibility of the components greatly influences the morphology, properties and end use. Generally, the miscibility of polymer blends can be estimated via the glass transition temperature[31] and melt viscoelasticity.[32] The visual observation with SEM is also an effective supplementary. Figure 1 shows the dependence of storage modulus (G') of the blends on the frequency at 190°C. It is clear that in low frequency region ($\omega < 0.046$ Hz), G' increases with increasing content of PLA and drops at a PLA content of 20 wt %. For FL20, G' is even smaller than that of neat PVDF, which can be explained by the concentration fluctuation and variation of interfacial area.[33,34] The increasing G' at low frequency for FL5, FL10, and FL15 is resulted from the increase of initial stress (interfacial interactions between PVDF and PLA) caused by the increasing volume fraction of PLA, while the decrease of G' in FL20 is ascribed to the decrease of interfacial area per unit volume that aroused by the coalescence of the PLA phase. At a low PLA content, the higher interfacial area per unit volume of the disperse phase leads to a stronger interfacial interaction; while the increase of domain size will reduce the interfacial area so that the interfacial interaction (adsorption) between PVDF and PLA decreases at higher PLA content. At high frequency region, neat PVDF exhibits the highest G' and the modulus of the blends decrease obviously with increasing PLA content which is caused by the phase separation of PVDF and PLA.[34]

The dependence of complex viscosity ($|\eta^*|$) on frequency for PVDF/PLA blends is shown in Figure 2. The complex viscosity for both pure PVDF and PVDF/PLA blends decreases with the frequency increasing, showing a shear-thinning behavior. The addition of the PLA causes slight decline of viscosity of the blends, which is much more evident at low frequencies.

Loss tangent (tan δ) is also used to characterize the viscoelasticity of materials and low value of tan δ indicates that the material exhibits relatively more solid-like behavior or elasticity. The tan δ curves of PVDF/PLA blends and pure components are displayed in Figure 3. It can be seen that tan δ decreases visibly with increasing content of PLA at low frequencies ($\omega < 0.046$ Hz), implying the effect of PVDF-PLA interfacial interaction on the relaxations of PVDF and PLA chains. At low frequencies, the blends have a lower tan δ than that of neat PVDF and PLA, whereas it rises with increasing content of PLA at high frequencies, which indicates PVDF-PLA interface interaction (adsorption) has been weakened due to the phase separation of PVDF and PLA.[34]

The Cole–Cole curve together with the SEM images was shown in Figure 4. It is well known that Cole–Cole curve is an effective characterization of two-phase structure of polymer blends.[35] It is evident that neat PVDF exhibits a visibly single arc, while the

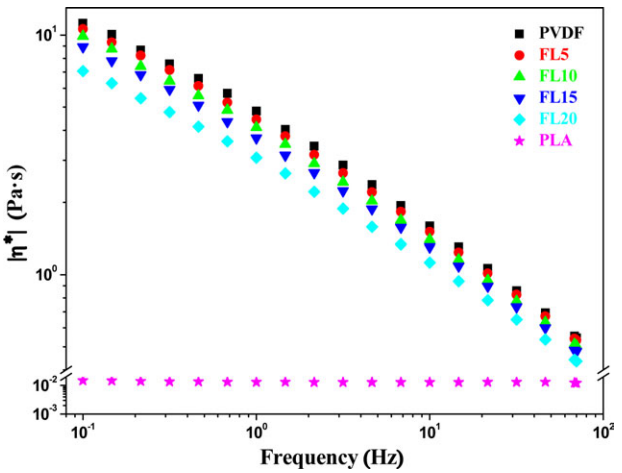

Figure 2. Dependence of complex viscosity ($|\eta^*|$) on frequency for PVDF/PLA blends. [Color figure can be viewed in the online issue, which is available at wileyonlinelibrary.com.]

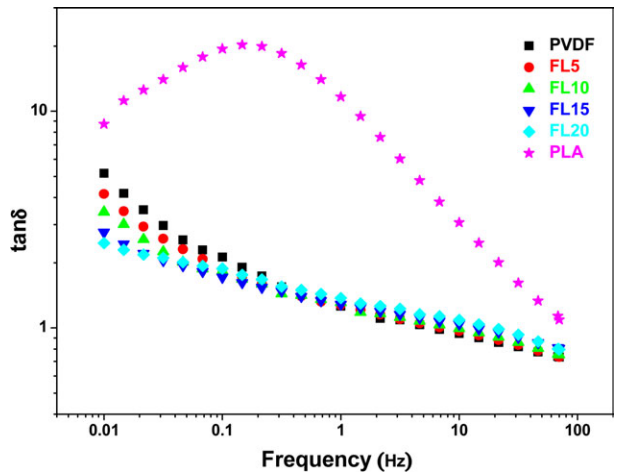

Figure 3. Dependence of loss tangent (tan δ) on frequency for PVDF/PLA blends. [Color figure can be viewed in the online issue, which is available at wileyonlinelibrary.com.]

arc gets more and more invisible with increasing PLA content for the blends, and disappears for FL20, which indicates two distinguishing relaxation mechanisms resulted from different internal structures.[35,36] In order to trace the reasons of the deviated relaxation behavior, SEM images and the mean size of dispersed phase are also included in Figure 4. The dominant morphology of PVDF/PLA blends is the typical sea-island morphology, and the size of dispersed phase increases with PLA content increasing. The average sizes of the PLA particles are 0.35 μm, 0.48 μm and 0.65 μm in FL5, FL10 and FL15, respectively. When 20 wt% PLA was introduced, the size of the dispersed phase increased to 1.26 μm which is much bigger than other blends. Consequently, it can be deduced that PVDF/PLA is an immiscible system based on the melt rheology and SEM characterizations.

Phase Transition

Molecular Vibration Spectrum. α- and β-phase PVDF exhibit distinct vibration bands in FTIR spectra and vibration bands at 530, 615, 765, 795, and 976 cm^{-1} are attributed to α-phase, while those at 510 and 840 cm^{-1} indicate the existence of β-phase.[13,14,18] To reveal the effect of stretching on the crystalline phase transition of PVDF in the blends, samples were stretched at 60, 80 and 100°C with a stretch ratio of 4. Figure 5 shows the FTIR absorption spectra of the unstretched samples and the samples stretched at different temperatures. It is clear that the unstretched blends only exhibit typical vibration bands of α-phase at 765, 795, and 975 cm^{-1} marked with small rhombuses in Figure 5(a) and there is no visible absorption band for β-phase PVDF. The inconspicuous absorption band at 755 cm^{-1} corresponds to the crystalline phase of PLA.[37] However, when the samples were stretched at 60°C which is close to the glass transition temperature of PLA, as shown in Figure 5(b), α-phase PVDF becomes unobvious and strong absorption band of β-phase PVDF marked with heart appears, indicative of the transition of α- to β-phase for PVDF. In addition, the absorption band of the crystalline phase of PLA at 755 cm^{-1} gets

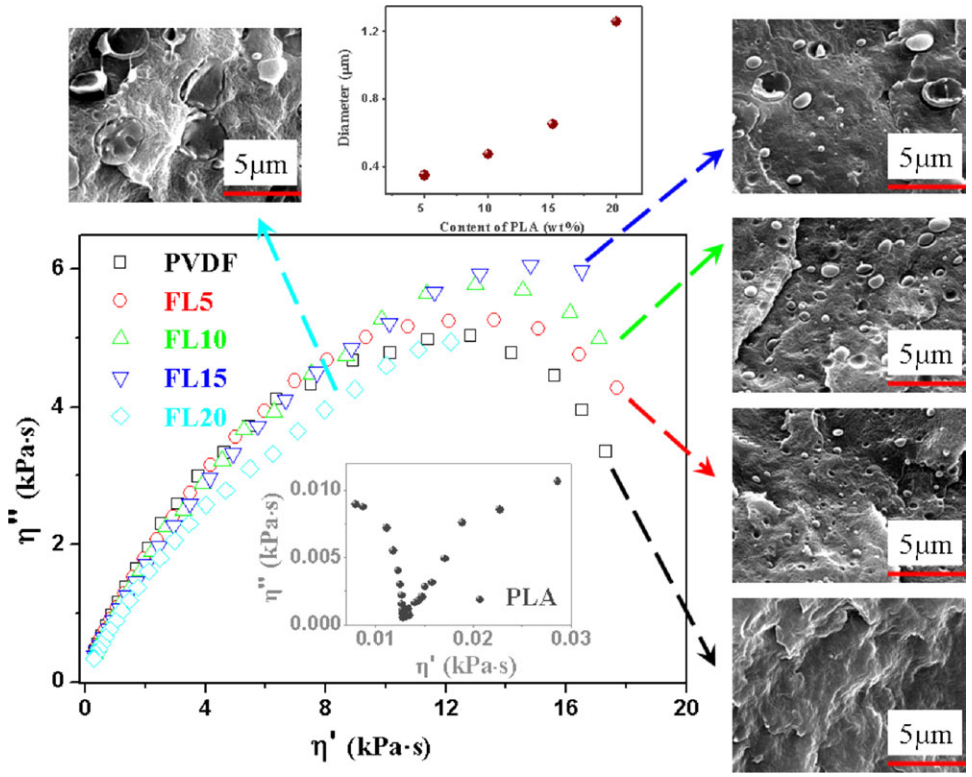

Figure 4. Cole–Cole curve and morphology of PVDF/PLA blends. [Color figure can be viewed in the online issue, which is available at wileyonlinelibrary.com.]

Applied Polymer SCIENCE

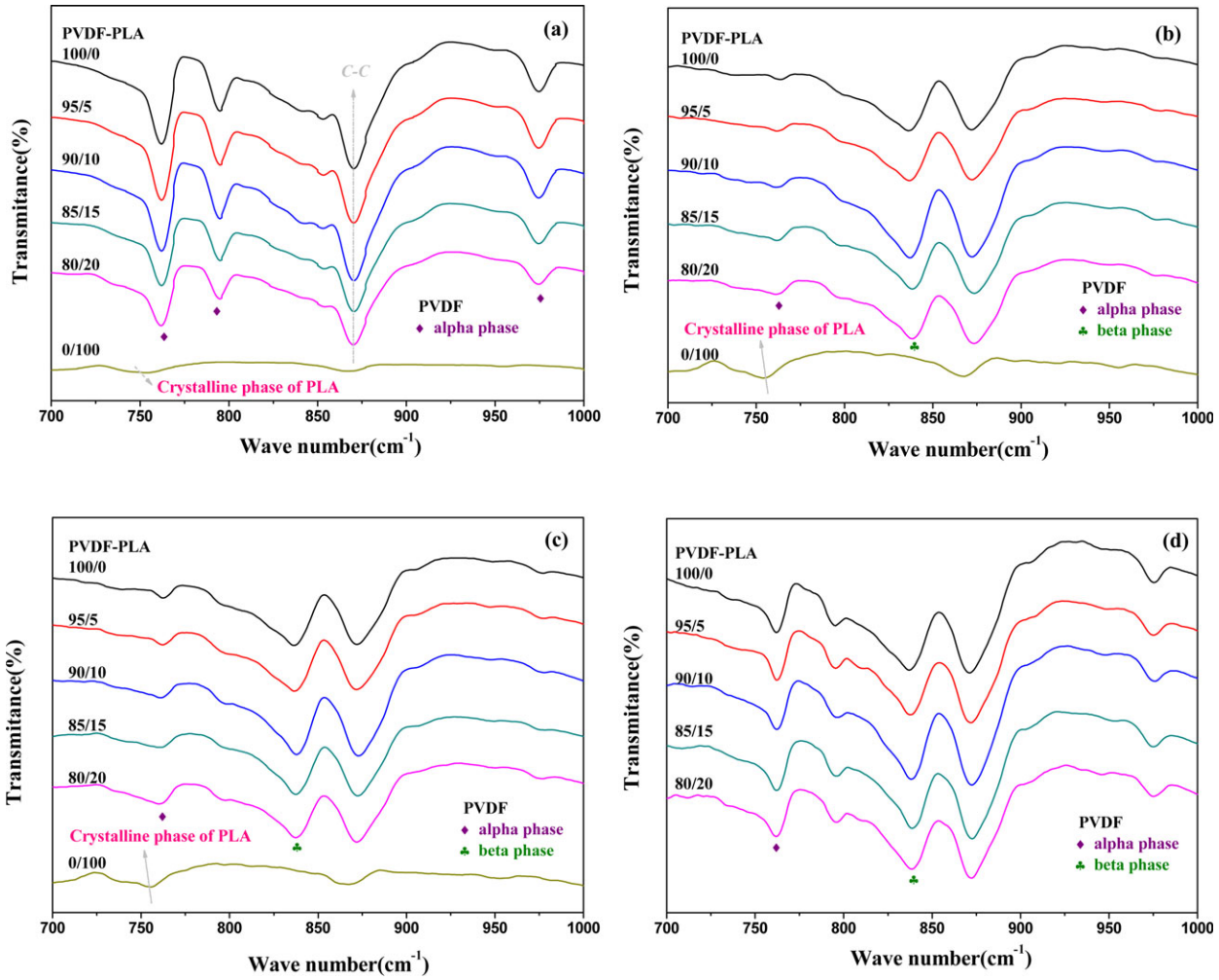

Figure 5. FTIR absorption spectra of (a) unstretched samples and samples stretched at (b) 60°C; (c) 80°C; (d) 100°C with a stretch ratio of 4 for PVDF/PLA blends. [Color figure can be viewed in the online issue, which is available at wileyonlinelibrary.com.]

more visible in Figure 5(b), which indicates that stretching also promotes the crystallization of PLA. This promotion can be also seen in Figure 5(c). Besides, both the band areas at 765 and 840 cm^{-1} increase slowly with increasing content of PLA. Similar results are also observed when the samples are stretched at 80°C [Figure 5(c)], but α-phase gets more obvious for the samples stretched at 100°C [Figure 5(d)]. These results thus reveal that mechanical stretching shows a considerable effect on the crystalline phase transition of PVDF in PVDF/PLA blends, and the transition is temperature-dependent.

To give an detailed description of the influence of temperature and PLA content on the phase transition of PVDF during stretching, the content of β-phase (F(β)) is calculated according to the following equation[13,14]

$$F(\beta) = \frac{X_\beta}{X_\alpha + X_\beta} = \frac{K_\beta}{(K_\beta + K_\alpha)A_\alpha + A_\beta} = \frac{A_\beta}{1.26A_\alpha + A_\beta} \quad (1)$$

in which X_α and X_β are the crystalline mass fraction of α- and β-phases and A_α and A_β correspond to the area under the absorption bands at 763 and 840 cm^{-1}, respectively. The absorption coefficients of $K_\alpha = 6.1 \times 10^4$ and $K_\beta = 7.7 \times 10^4$ cm^2/mol at 763 and 840 cm^{-1}, are features of α- and β-phases.[13,14] In Figure 6, the dependence of F(β) on the stretching temperature and PLA content is presented. It is clear that the incorporation of PLA shows a positive effect on the content of β-phase of PVDF when PLA content is no more than 15 wt % for the samples stretched at the three different temperatures, and there is a maximum value of F(β) with the addition of 10 wt % PLA, but an significant decline of F(β) is encountered in the blends containing 20 wt % PLA. Comparatively speaking, relatively higher F(β) is achieved for the samples stretched at 60°C compared with those stretched at 80 and 100°C.

It is known that the α- to β-phase transition of PVDF relates to the stretching conditions, including stretching speed, ratio and temperature. The reported optimal stretching conditions to achieve the highest content of β-phase were 80–90°C and a stretching rate of ca. 138 mm/min.[12] The difference in the optimal conditions can be ascribed to two factors. For one thing, the stress relaxation during stretching is weaker at a higher stretching rate.[13] Whereas the drawing rate used in this work is 5 mm/min, which is much lower than those reported in

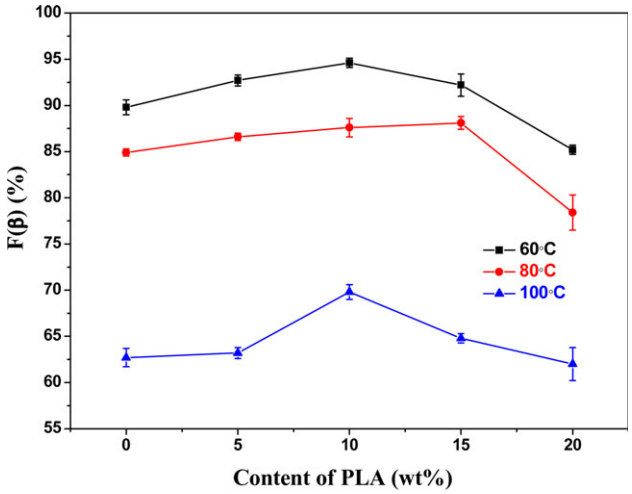

Figure 6. Content of β-phase as a function of PLA content for PVDF/PLA blends stretched at different temperatures. [Color figure can be viewed in the online issue, which is available at wileyonlinelibrary.com.]

literatures.[12–14] For another, Gregorio et al.[38] pointed out that the optimal crystallization temperature of β-phase is 60 °C or slightly lower and the deformation at low temperature provides more effective stress transfer to the crystals due to the higher viscosity, while the viscosity decreases with the temperature increasing. As a result, the samples stretched at 60°C are more prone to exhibits the highest F(β) based on the advantages of the better stress transfer and lower energy barrier for crystalline phase transition. Because the glass transition temperature of PLA is in the vicinity of 60°C, the highest viscosity of the PLA phase can be obtained at 60°C. When the samples are stretched at 100°C, F(β) decreases sharply compared with that of 60 and 80°C.

Compared with the F(β) of neat PVDF, FL10 exhibits a little higher F(β) no matter what the stretching temperature is. It implies that both the stretching temperature and PLA content can affect the α- to β-phase transition of PVDF in the blends. Specially, for neat PVDF, stretching temperature plays a significant role in the α- to β-phase transition, because the energy barrier is the predominated factor; while for the blends, the sea-island structure of the blends depending on the content of PLA also plays a critical role in the crystalline phase transition of PVDF. This can be attributed to the fact that low PLA content can promote the necking of PVDF due to the deformation and tearing of PLA in the vicinity of phase interface. However, when high content, for example, 20 wt% of PLA, was introduced, the strength of the blends will decrease obviously (as can be revealed in Figure 1 that with the addition of 20 wt% PLA, the storage modulus decrease) and the stress transfer from the amorphous region to crystalline region will be weakened, so the α- to β-phase transition weakens.

WAXD. In WAXD patterns, α-phase of PVDF exhibits typical diffraction peaks at $2\theta = 17.6$, 18.3, 19.9, 26.6, and 35.7°, corresponding to the (100), (020), (110), (021), and (200) lattice planes, and diffraction peak at $2\theta = 20.5$, 36.6° corresponds to the (110/200), (020/101) planes of β-phase,[14,20] while the peak at $2\theta = 36.3°$ corresponds to (200) lattice plane of γ phase.[39,40] PLA shows a typical diffraction peak of (200/110) plane at $2\theta = 16.4°$.[8] Figure 7 represents the WAXD patterns of PVDF/PLA blends. As shown in Figure 7(a), the unstretched samples exhibit typical diffraction peaks of α phase of PVDF. With the addition of PLA, the intensity of these peak increases visibly. While neat PLA shows only a camel peak indicating that it is amorphous or the amount of crystalline structure is too small to be traced. However, the diffraction peaks of α phase of PVDF vanish and those of β-phase of PVDF occur when the samples are stretched at 60 °C as shown in Figure 7(b). A broad diffraction peak of PLA occurs at $2\theta = 15.9°$, also indicating that the stretching promoted the crystallization of PLA. Noted that whether the diffraction peak of PVDF around $2\theta = 36.3°$ is from β- or γ- phase of PVDF is still in dispute.[14,39,40]

When the samples are stretched at 60 and 80°C, the intensity of diffraction peaks of β-phase is connected with the PLA loading level. For sample FL5, FL10, and FL15, the intensity of the diffraction peak at $2\theta = 20.5°$ is a little stronger than that of PVDF. Particularly, the intensity of diffraction peak for FL10 is the most significant whereas it is weakest for FL20. Interestingly, there is no diffraction peak at $2\theta = 16.5°$ for PLA in the blends stretched at 60°C, while the diffraction peak of PLA crystals visibly appears when the samples are stretched at 80°C, and gets stronger with the increasing PLA content. Neat PLA stretched at 80°C exhibits two diffraction peaks at $2\theta = 16.5°$ and 22.5° ((015) crystal plane of α PLA),[41] as shown in the inset of Figure 7(c). But in the blends only a single diffraction peak of PLA crystals can be observed. Thus, it can be concluded that the stretching at higher temperatures indeed promotes the crystallization of PLA, especially at 100°C as shown in Figure 7(d). The PLA sheet itself cannot be stretched stably at 100°C, so the data of PLA are not included in Figure 7(d). However, owing to the different crystallization temperatures and crystallization rates between PVDF and PLA, the confinement of PVDF to the crystallization of PLA is inevitable. In addition, the diffraction peak of α-phase PVDF appears at $2\theta = 18.4°$ again, indicating that higher temperature stretching goes against the conversion from α- to β-phase.

To sum up, the phase transition of PVDF in PVDF/PLA blends under uniaxial stretching depends on both stretching temperature and PLA content. Compared with neat PVDF, the addition of PLA improves the formation of β-phase PVDF when the content of PLA is no more than 15 wt % for the samples stretched at three different temperatures. However, when 20 wt % PLA was introduced, the content of β-phase PVDF decrease obviously. Also, the stretching process promotes the crystallization of PLA due to the alignment of PLA chains, and a greater promotion effect is observed when the samples are stretched at higher temperatures.

Thermal Properties. In Figure 8, the crystallization and melting behavior of the unstretched PVDF, PLA, and PVDF/PLA blends are shown. It can be seen that the crystallization peak temperatures (T_{CP}s) of PVDF and PLA are considerably different and the addition of PLA shifts the crystallization peak temperatures (T_{CP}s) of PVDF in the blends to lower temperatures slightly. Besides, the exothermic and endothermic peaks of neat PLA clearly appear in Figure 8, while it is unconspicuous in the

Applied Polymer SCIENCE

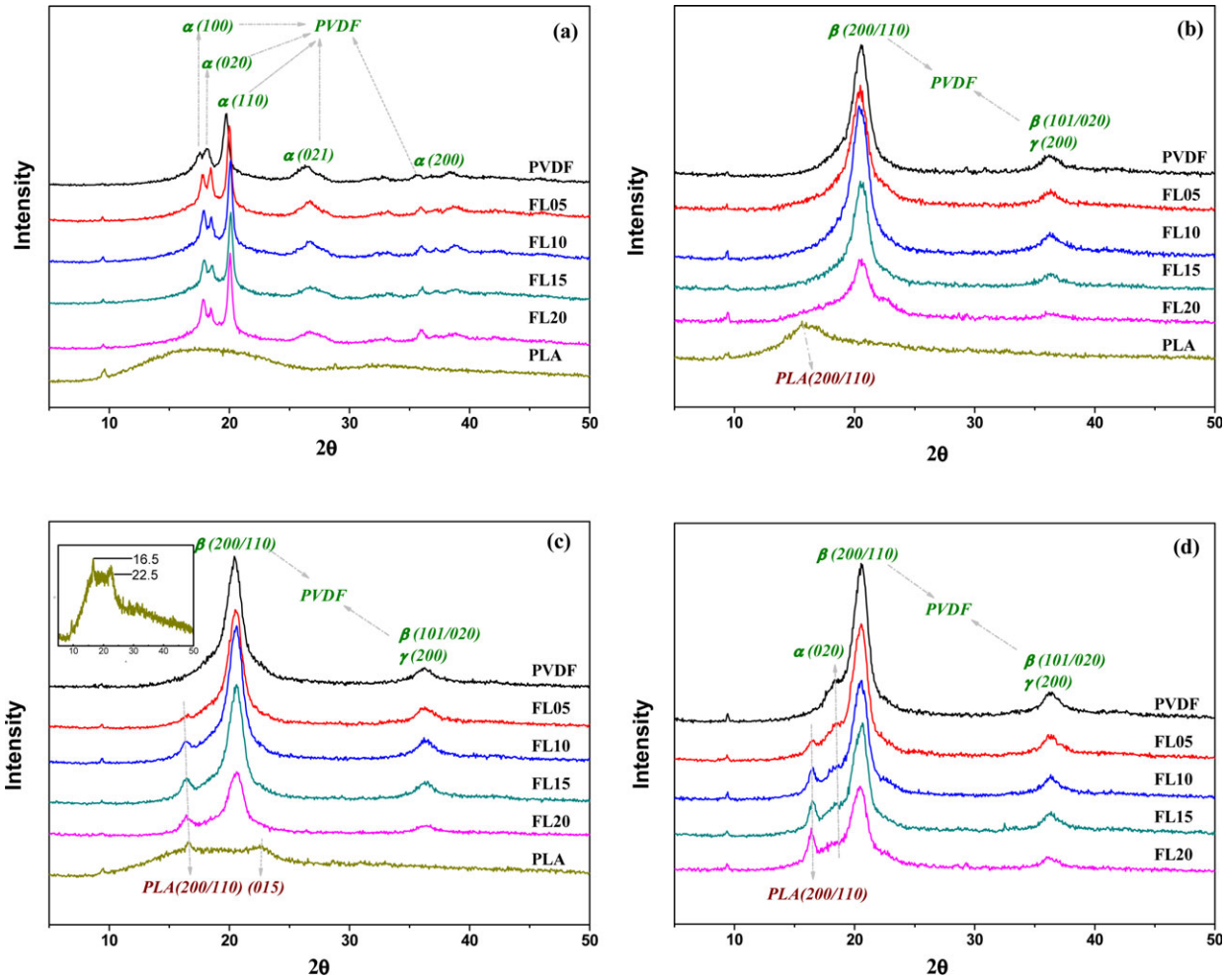

Figure 7. WAXD patterns of (a) unstretched samples and samples stretched at (b) 60°C; (c) 80°C; (d) 100°C of PVDF/PLA blends. [Color figure can be viewed in the online issue, which is available at wileyonlinelibrary.com.]

blends. This is consistent with the results shown Figures 5(a) and 7(a) to some degree.

The degree of crystallinity of PVDF in the blends can be measured by the crystallization enthalpy (ΔH_C).[42–44] T_{CP} and ΔH_C listed in Table I. The crystallinity of PVDF and PLA is calculated from the following equation:

$$X_C = \Delta H_{cf} / \Delta H_f^0 \phi \quad (2)$$

in which X_C is the degree of crystallinity, ΔH_{cf} is the measured crystallization enthalpy from the DSC trace, ΔH_f^0 is the fusion enthalpy of the 100% crystallized material (ΔH_f^0 is 104.6 J/g for PVDF,[19] and 93 J/g for PLA[45]), and ϕ is the weight fraction of PVDF or PLA.

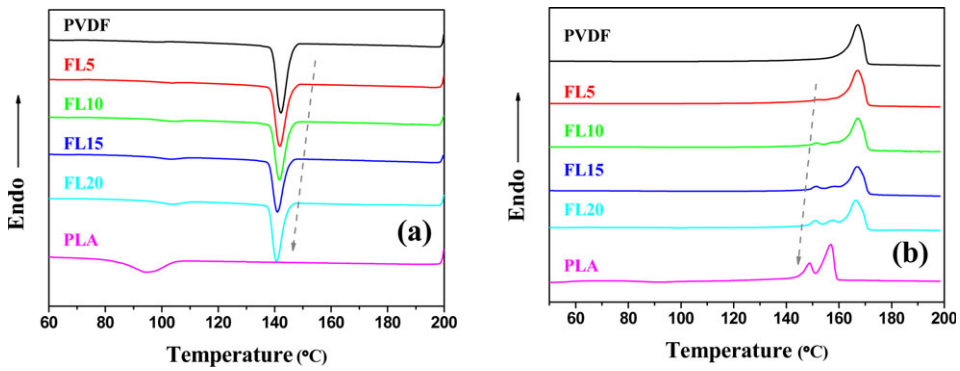

Figure 8. DSC heat flows of (a) cooling and (b) heating curves of unstretched PVDF, PLA, and PVDF/PLA blends. [Color figure can be viewed in the online issue, which is available at wileyonlinelibrary.com.]

Table I. Crystallization Parameters of PVDF, PLA, and PVDF/PLA Blends

Samples	T_{CP} (°C)	ΔH_C (J/g)	X_C (%)
PVDF	142.15	49.22	47.06
FL5	141.76	46.12	46.41
FL10	141.55	41.08	43.64
FL15	140.92	33.74	37.95
FL20	140.57	35.34	42.23
PLA	94.47	27.76	29.85

From Table I, it can be seen that the T_{CP}, ΔH_C, and X_C of the blends decrease with increasing content of PLA, which demonstrates that the addition of PLA restrains the crystallization of PVDF due to the decreased mobility of PVDF chains caused by interfacial interaction between PVDF and PLA. Similar results have been also reported in literatures.[30]

For the melting behavior, PLA shows double melting behavior due to different lamella thickness of the crystals and PVDF shows a single melting peak. With the addition of PLA, no difference can be seen for the melting peak temperature of PVDF, but the melting peaks of PLA is more and more visible with the increasing content of PLA.

The results of FTIR molecular vibration spectrum and wide angle X-ray diffraction patterns have demonstrated that uniaxial stretching causes the α- to β-phase transition of PVDF, and promotes the crystallization of PLA. Here, the melting behaviors of unstretched samples and samples stretched at different temperatures are compared in Figures 8 and 9.

Ince-Gunduz et al.[46] found that γ-phase of PVDF has the melting temperature of ca.174 °C, which is higher than that of α-phase, 168°C. Gregorio et al.[47] found that the β-phase PVDF shows similar melting temperature with α-phase. Zhao et al.[48] found that the melting peak temperature of β-phase PVDF in PVDF/PMMA blends produced by solution casting is about 163°C, which is lower than that of neat PVDF (α phase). In fact, many factors, such as experimental instruments and conditions, raw material and error in calculating the peak temperature, can result in the difference in the melting peak temperature.

In Figure 9(a), the melting behaviors of unstretched samples are provided for comparison. It is clear that there are two melting peaks of neat PVDF at about 163 and 169°C, marked as T_{m2} and T_{m3}, respectively. The melting peak of PLA at 156°C, labeled as T_{m1}, becomes more and more obvious with increasing content of PLA. Besides, the glass transition temperature of PLA appears at 60°C obviously, which confirms the immiscibility between PLA and PVDF, which has also been found by Li et al. in PVDF/PLLA blends.[29] For stretched neat PVDF, there is a strong peak (labeled as T_2) at 163°C and a weak shoulder (labeled as T_3) locates at 168°C, respectively. Meanwhile, the melting peak of PLA shifts to 153°C (labeled as T_1), and with the increasing PLA content, it becomes more obvious.

Different from the melting peaks of unstretched PVDF in Figure 9(a), the location of melting peaks for PVDF in Figure 9(b) has inversed. There is a shoulder following the dominated melting peak at 163°C. Similar phenomenon can be observed from the changes of melting peaks of other samples in Figure 9(c,d). When the content of PLA or the stretching temperatures are increased, the shoulder becomes more visible, but the main melting peak located at 163°C seems to be unchanged. From the results of FTIR and WAXD, it can be found that the β-phase is the dominant crystalline phase for the stretched PVDF and PVDF/PLA blends and there is a small amount of α-phase left. Thus it can be concluded that the T_2 is the melting temperature peak of β-phase PVDF crystals, while that of α-phase corresponds to T_3. The melting temperature of β-phase PVDF stated here is lower than that of α-phase PVDF due to the smaller lamella thickness or imperfection of crystals, because the β-crystals are mainly resulted from the rearrangement of the destroyed α-crystals and the aligned chains of the amorphous zone. It is necessary to note that the T_3 gets stronger with the stretching temperature, indicating the increment of the α-phase caused by the stretching at higher temperature.

Discussion

As we know, during uniaxial stretching a reduced thickness section appears and the necking region forms in the sample.

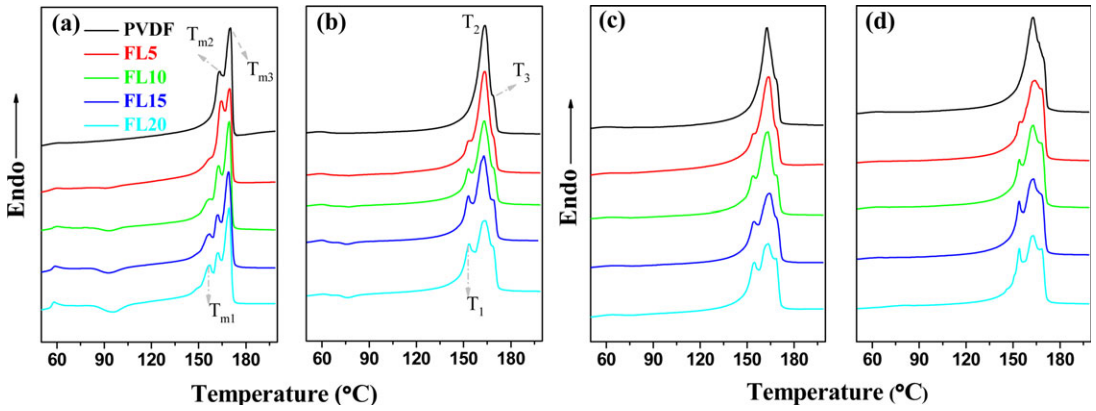

Figure 9. DSC heating curves of samples (a) unstretched, and stretched at (b) 60°C, (c) 80°C, and (d) 100°C. [Color figure can be viewed in the online issue, which is available at wileyonlinelibrary.com.]

Applied Polymer SCIENCE

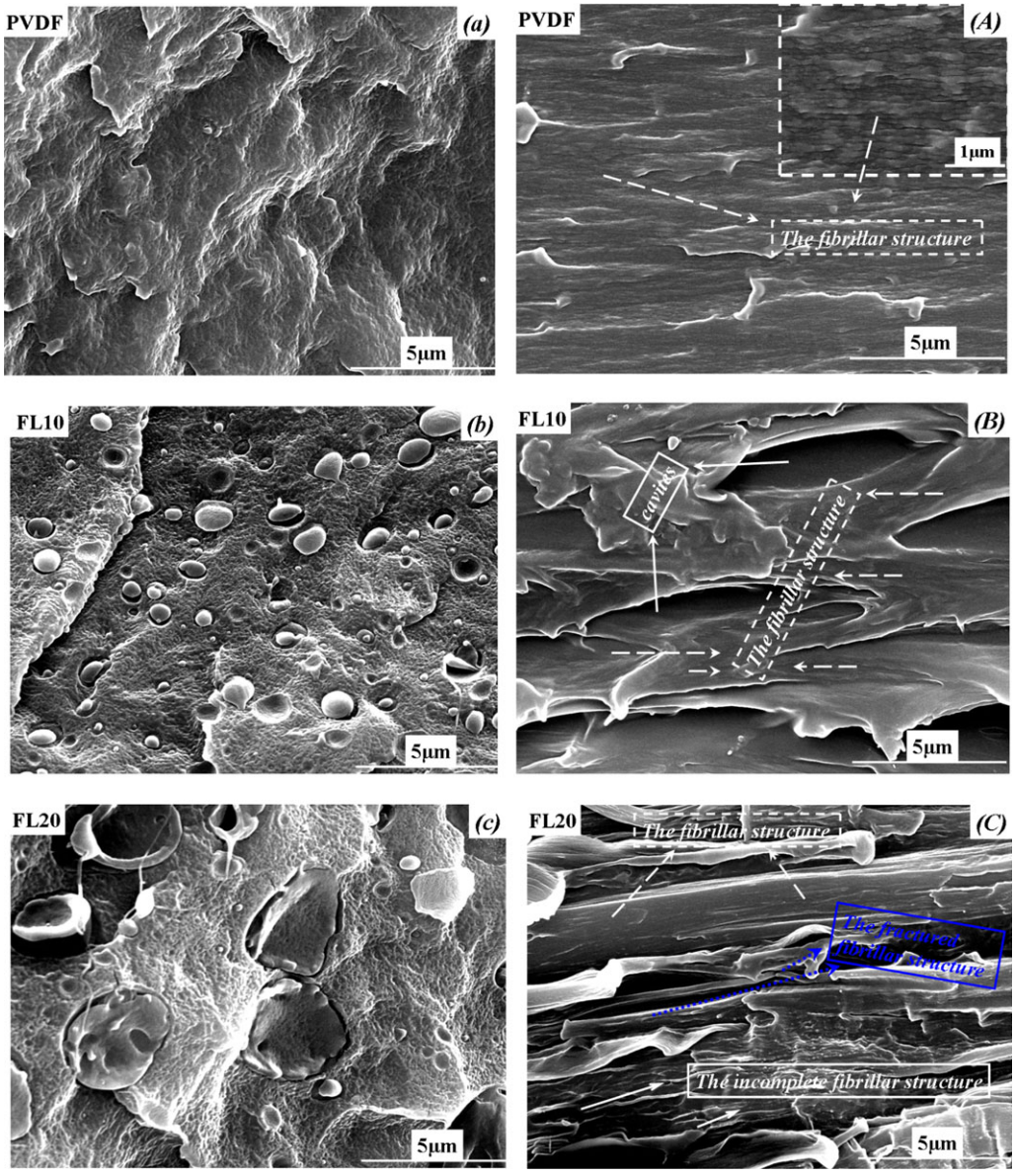

Figure 10. Morphologies of fractured surfaces of PVDF, FL10 and FL20 before and after stretching. The images labeled with (a), (b), and (c) in the top right corner of the image are those before the stretching. Oppositely, the samples stretched are marked by capital letters. The fracture surfaces of the stretched samples are parallel to the stretch direction. [Color figure can be viewed in the online issue, which is available at wileyonlinelibrary.com.]

Afterwards, the neck spreads along the stretching direction on both sides. The α- to β-phase transformation occurs at the location where necking region commences. Necking causes the transformation form spherulitic structure to micro fibrillar one and the small blocks of lamella are torn away form original lamella to form a fibrillar structure of crystallites.[12–14] This transformation has also been revealed in PVDF/PLA blends studied in this work. The fracture surface morphologies of PVDF and PVDF/PLA blends before and after stretching are shown in Figure 10. Note that the samples stretched at 80°C are opted to give a mechanism analysis.

It is clear that visible fibrillar structure appears in stretched PVDF sample compared with the unstretched sample, which can be more clearly revealed by the inset of PVDF in Figure 10(a). These fibrillar structures derive from the transformation from spherulitic structure to a micro-fibrillar structure. While for PVDF/PLA blends, the mechanism is more complex because of the existence of PLA phase. The lower storage modulus and viscosity of PLA in Figures 1 and 2, compared with those of PVDF, show that PLA is much more intended to deform. The deformation of PLA generates many cavities owing to the destroying of the PLA dispersed phase during stretching, as shown in Figure 10(b). As a result, the local neck formation for the PVDF matrix is easier in the blends owing to the heterogeneous stress distribution. Besides, PVDF-PLA interface interaction (adsorption) will be weakened during the stretching under different temperatures. The weak interface adsorption will be a defect, which induces the local neck formation and accelerate deformation of PVDF matrix, Consequently, the α- to

β-phase transition is facilitated. It is visible that the size of dispersed PLA particles exhibits an increase of 4 orders of magnitude after being stretched for FL10. Besides, the fibrillar structure of PVDF located in the vicinity of seriously-deformed PLA particles can be found in Figure 10(b,c). However, the destroying of PLA phase is disadvantageous to the stress transfer of PVDF when excessive PLA is incorporated, such as the case for the blends containing 20 wt% PLA. Obviously, stretching induced the separation between PVDF and PLA phases due to extraordinary big cavities and poor interface adsorption, which leads to the fracture of local PVDF phase around PLA phase. It harms the necking formation of PVDF definitely, together with the emergence of incomplete fibrillar structure of PVDF. This can be seen from the fractured morphologies of PVDF marked in Figure 10(c) and other micrographs are not provided here.

The different sea-island structures in the blends, determined by the content and PLA disperse phase and of course the molecular parameters of both components, response differently during the stretching process. With the addition of small amount of PLA, the formation of necking of the matrix will be promoted and the fibrillization of PVDF will be enhanced due to the locally increased deformability of PVDF induced by the deformation PLA, as a result the arrival of the required 400% strain will emerge in advance. The stress acted on the PVDF increases with the increasing content of PLA due to the enhanced deformability caused by increased size of PLA and the necking formation will be accelerated at the same time. It leads to the increment of β-phase PVDF in the PVDF/PLA blends. While with further increase of PLA content in the blends, such as 20 wt % PLA, the size of the PLA dispersed phase is much bigger than that of the other blends with a PLA content no more than 15 wt %. The deformation of PLA is very serious as shown in Figure 10(c) due to large size dispersed phase, which results in the fractures of PLA phase and PVDF phase during stretching. The higher stretching temperature makes the fracture easier. The seriously destroying of PLA phase is disadvantageous to the stress transfer of PVDF. Of course, it is not beneficial to the crystalline phase transition of PVDF.

Likewise, the role of PLA in the deformation and crystalline phase transition of PVDF during the stretching at other temperatures is the same with that in the samples stretched at 80°C. It is known that orientation and relaxation of the polymers are dependent on the temperature and loading level of applied stress. Under the same applied strain, the orientation of samples relies on the deformation temperature apparently. It was reported that 65°C is optimal to generate the α- to β-phase transformation of PVDF.[13] When the samples are stretched at 60°C, the temperature is obviously more suitable for the crystalline phase transformation, because at the lower temperature, the viscosity of the material is high and the stress introduced by deformation is sufficiently high to destroy crystals. As stated, PLA is easier to deform than that of PVDF, so the addition of low content of PLA can promote the local deformation of PVDF and accelerate the forming of neck region. The local deformation will generate heterogeneous deformation of PVDF so that the efficiency of α- to β-phase transition improves. At elevated stretching temperature, the deformation of the samples speeds up due to the increased mobility of polymer chains, resulting in more efficient destroying of α-crystals of PVDF and more orientation of PVDF chains in the amorphous zone, which are advantageous to rearrange the PVDF chains into all trans planar zigzag conformation. At the same time, α-crystals of PVDF align along the drawing direction, and the relaxations of PVDF and PLA accelerate at a higher temperature as well, which are disadvantageous to the α- to β-phase transition of PVDF. Consequently, there is a competition between the orientations of α-crystals and the transformation from α- to β-crystals of PVDF, and the competition between the damage of α-crystals and the deformation and fracture of PLA and PVDF phase can not neglected. So, there is little difference in the F(β) for the samples stretched at different temperatures, and the effect of PLA content on the crystalline phase transition of PVDF is a little more complex.

CONCLUSIONS

The effect of PLA on the crystalline phase transition of PVDF from α to β under uniaxial stretching was studied. Because PVDF and PLA are immiscible, typical sea-island structure was formed, which facilitate the necking and the transition of α- to β-crystals of PVDF due to the local stress distribution during stretching. The transition is temperature-dependent and affected by the content of PLA. Relatively higher F(β) is achieved for the samples stretched at 60°C compared with those stretched at 80°C and when the samples are stretched at 100°C, F(β) decreases sharply. F(β) increases slightly when the sample with a PLA content no more than 15 wt % are stretched at 60, 80, and 100°C, and exhibits the highest F(β) at a PLA content of 10 wt %. The mechanism of the crystalline phase transition of PVDF during the stretching can be interpreted from energy barrier of the transition of α to β and the phase morphological structures in the blends. Also, there is a confinement effect of PVDF on the crystallization of PLA due to the visible difference in the crystallization temperature and uniaxial stretching contributes to the crystallization of PLA.

ACKNOWLEDGMENTS

The authors are grateful to the National Natural Science Foundation of China (Grant Nos. 50973074 and 51073110), Fok Ying Tung Education Foundation (Grant no.: 122022) and the Fundamental Research Funds for the Central Universities (Grant no. 2011SCU04A03) for the financial support.

REFERENCES

1. Strohmeier, W.; Frank, W. *Colloid. Polym. Sci.* **1982**, *260*, 937.
2. Rao, I.; Rajagopal, K. *Int. J. Solids. Struct.* **2001**, *38*, 1149.
3. Bao, R. Y.; Ding, Z. T.; Zhong, G. J.; Yang, W.; Xie, B. H.; Yang, M. B. *Colloid. Polym. Sci.* **2012**, *290*, 261.
4. Krumova, M.; Karger-Kocsis, J.; Baltá-Calleja, F.; Fakirov, S. *J. Mater. Sci.* **1999**, *34*, 2371.
5. Yokouchi, M.; Sakakibara, Y.; Chatani, Y.; Tadokoro, H.; Tanaka, T.; Yoda, K. *Macromolecules.* **1976**, *9*, 266.

6. Miri, V.; Persyn, O.; Lefebvre, J.; Seguela, R.; Stroeks, A. *Polymer* **2007**, *48*, 5080.
7. Kokturk, G.; Piskin, E.; Serhatkulu, T.; Cakmak, M. *Polym. Eng. Sci.* **2002**, *42*, 1619.
8. Zhang, X.; Schneider, K.; Liu, G.; Chen, J.; Brüning, K.; Wang, D.; Stamm, M. *Polymer* **2011**, *52*, 4141.
9. Lando, J.; Olf, H.; Peterlin, A. *J. Polym. Sci.: Part A.* **1966**, *4*, 941.
10. Matsushige, K.; Nagata, K.; Imada, S.; Takemura, T. *Polymer* **1980**, *21*, 1391.
11. Lund, A.; Hagstrom, B. *J. Appl. Polym. Sci.* **2010**, *116*, 2685.
12. Sajkiewicz, P.; Wasiak, A.; Gocłowski, Z. *Eur. Polym. J.* **1999**, *35*, 423.
13. Salimi, A.; Yousefi, A. *Polym. Test.* **2003**, *22*, 699.
14. Mohammadi, B.; Yousefi, A. A.; Bellah, S. M. *Polym. Test.* **2007**, *26*, 42.
15. Sencadas, V.; Gregorio, R. Jr; Lanceros-Méndez, S. *J. Macromol. Sci.: Part B.* **2009**, *48*, 514.
16. Ke, K.; Wang, Y.; Zhang, K.; Luo, Y.; Yang, W.; Xie, B. H.; Yang, M. B. *J. Appl. Polym. Sci.* **2012**, *125*, 49.
17. Lu, F.; Hsu, S. *Polymer.* **1984**, *25*, 1247.
18. Gregorio, R.; Borges, D. S. *Polymer* **2008**, *49*, 4009.
19. Buckley, J.; Cebe, P.; Cherdack, D.; Crawford, J.; Ince, B. S.; Jenkins, M.; Pan, J.; Reveley, M.; Washington, N.; Wolchover, N. *Polymer* **2006**, *47*, 2411.
20. Tang, X. G.; Hou, M.; Ge, L.; Zou, J.; Truss, R.; Yang, W.; Yang, M. B.; Zhu, Z. H.; Bao, R. Y. *J. Appl. Polym. Sci.* **2012**, *125*, 592.
21. Li, Y.; Kaito, A.; Horiuchi, S. *Macromolecules* **2004**, *37*, 2119.
22. Li, Y.; Iwakura, Y.; Shimizu, H. *Macromolecules* **2008**, *41*, 3396.
23. Li, Y.; Shimizu, H.; Furumichi, T.; Takahashi, Y.; Furukawa, T. *J. Polym. Sci.: Polym. Phys.* **2007**, *45*, 2707.
24. Gregorio, R. Jr. Nociti, N. *J. Phys. D.: Appl. Phys.* **1995**, *28*, 432.
25. Madhavan Nampoothiri, K.; Nair, N. R.; John, R. P. *Bioresource. Technol.* **2010**, *101*, 8493.
26. Harrison, J.; Ounaies, Z. Polymers, Piezoelectric. In Encyclopedia of Smart Materials; Schwartz, M.; Wiley: New York, **2002**, 162.
27. Fukada, E. *IEEE T Dielect El In* **2006**, *13*, 1110.
28. Ikada, Y.; Shikinami, Y.; Hara, Y.; Tagawa, M.; Fukada, E. *J. Biomed. Mater. Res.* **1996**, *30*, 553.
29. Kaito, A.; Iwakura, Y.; Li, Y.; Shimizu, H. *J. Polym. Sci.: Polym. Phys.* **2008**, *46*, 1376.
30. Chen, H. C.; Tsai, C. H.; Yang, M. C. *J. Polym. Res.* **2011**, *18*, 319.
31. Lu, X.; Weiss, R. *Macromolecules* **1992**, *25*, 3242.
32. Kapnistos, M.; Hinrichs, A.; Vlassopoulos, D.; Anastasiadis, S.; Stammer, A.; Wolf, B. *Macromolecules* **1996**, *29*, 7155.
33. Zhang, Z.; Zhang, H.; Yang, Y.; Vinckier, I.; Laun, H. *Macromolecules* **2001**, *34*, 1416.
34. Niu, Y.; Yang, L.; Shimizu, K.; Pathak, J. A.; Wang, H.; Wang, Z. *J. Phys. Chem. B.* **2009**, *113*, 8820.
35. Chopra, D.; Kontopoulou, M.; Vlassopoulos, D.; Hatzikiriakos, S. G. *Rheol. Acta.* **2002**, *41*, 10.
36. Wu, D.; Zhang, Y.; Zhang, M.; Zhou, W. *Eur. Polym. J.* **2008**, *44*, 2171.
37. Garlotta, D. *J. Polym. Environ.* **2001**, *9*, 63.
38. Gregorio, R.; Ueno, E. *J. Mater. Sci.* **1999**, *34*, 4489.
39. Esterly, D. M.; Love, B. J. *J. Polym. Sci.: Polym. Phys.* **2004**, *42*, 91.
40. Almasri, A. Master of Science Thesis: Texas A&M University. **2006**.
41. Lai, W.; *J. Phys. Chem. B.* **2011**, *115*, 11029.
42. Asadinezhad, A.; Yavari, A.; Jafari, S.; Khonakdar, H.; Böhme, F.; Hässler, R. *Polym. Bull.* **2005**, *54*, 205.
43. Dai, S.; Ye, L. *Polym. Adv. Technol.* **2008**, *19*, 1069.
44. Atanase, L. I.; Glaied, O.; Riess, G. *Polymer* **2011**, *52*, 3074.
45. Li, Y.; Wang, Y.; Liu, L.; Han, L.; Xiang, F.; Zhou, Z. *J. Polym. Sci.: Polym. Phys.* **2009**, *47*, 326.
46. Ince-Gunduz, B. S.; Alpern, R.; Amare, D.; Crawford, J.; Dolan, B.; Jones, S.; Kobylarz, R.; Reveley, M.; Cebe, P. *Polymer* **2010**, *51*, 1485.
47. Gregorio, R.; Cestari, M. *J. Polym. Sci.: Polym. Phys.* **1994**, *32*, 859.
48. Zhao, X.; Chen, S.; Zhang, J.; Zhang, W.; Wang, X. *J. Cryst. Growth* **2011**, *328*, 74.